Design of an Optimized Distal Optic for Non Linear Endomicroscopy

Claire Lefort[1], Hussein Hamzeh[2], Liu Wei[2], David Sevrain[2], Philippe Leproux[1],
Frédéric Pain[2] and Darine Abi Haidar[2,3]

[1]Laboratoire XLIM, UMR 7252, CNRS, F-87060 Limoges, France
[2]Laboratoire IMNC, UMR 8165- Université Paris-Sud, Orsay, France
[3]Université Paris 7-DENIS DIDEROT, F-75012 Paris, France

Keywords: Nonlinear Endomicroscopy, Double-Clad Fibre, GRIN Lens, Zemax Simulations.

Abstract: The development of a nonlinear endomicroscope is justified by the need for a non-invasive diagnosis tool to assess at the cellular level, *in vivo* and *in live* the presence of pathologies like cancer in a patient body. To do so, an important effort has to be made in the miniaturization of the distal head of the endoscope. We report in this paper our work on the characterization of a commercial gradient index (GRIN) lens, especially its possible fluorescence emission and ability to image biological structures. We show that the fluorescence of the peripheral glue of the GRIN lens does not have impact on the fluorescence images but can lead to perturbations to measure fluorescence lifetime and emission spectrum. The axial and lateral resolutions are obtained by imaging 1 μm diameter gold beads. The results show a good agreement with values from the literature. Finally, we simulate an endomicroscope combining an appropriate double-clad fibre (DCF) with the GRIN lens and a tubular piezoelectric scanner (PZT) scanning head. Variations of parameters values like fibre tilt angle and distance between the DCF and the GRIN lens allow to discuss on the performances of this device in terms of working distance (WD), magnification, field of view (FOV) and coupling efficiency.

1 INTRODUCTION

Cancer is a family disease where abnormal cells are proliferating. It is becoming more and more widespread in the world. Cancer treatment is a ticklish issue, depending on the development of the cancerous tumour and its localisation in the patient's body. Nowadays, the main hope of curing this illness lies in surgery, often completed by chemical treatments or radiotherapy (Miller, 1981). If this global process is applied in the early stages of the disease, the chances to heal a patient and extends his hope of life considerably increase. Nevertheless, surgery is a very invasive operation and there still exists a risk of relapse associated with a new proliferation of cancerous cells in the treated area. This may be due to a non-complete removal of all the cancerous cells, despite the use of combined modality therapies.

Starting from this alarming observation, particularly true in the case of cancers where it is not possible to remove a large part of the tissues around the cancer area like the brain cancer, there is an need for a tool enabling a fast and accurate discrimination between cancerous and healthy cells.

A way to achieve this goal consists in the development of an endoscope with a microscopic resolution. The first endomicroscopes, now clinically used, are based on the confocal principle with an excitation laser source in the visible range (Salaün, 2010). This device allows to image endogenous tissue components like elastin, *in vivo* and *in real time.* However, some drawbacks can be underlined, such as an imaging depth limited to at a few tens of micrometres inside the target tissues, mainly due to the strong scattering properties of biological tissues, as well as the small number of mean contrasts available from endogenous fluorescent proteins under linear excitation.

To overcome this limitation, the current research on endomicroscopy aims at developing two-photon fluorescence (2PEF) imaging with femtosecond pulse (150fs) excitation at high excitation rate (80MHz) in the infrared (NIR) range (GU, 2014). The interest of nonlinear imaging technique compared to the confocal imaging is justified not only by an increase in imaging depth due to IR excitation (Cosignani 2012) but also by the availability of a new mean of contrast thanks to the second harmonic generation emitted by non-centro-

symmetrical structures as collagen. This fact, combined to the absence of confocal pinhole due to the intrinsic localisation of the nonlinear phenomenon in the focal plane of the focusing device, promote a deeper imaging depth within a few hundreds of micrometres

While nonlinear microscopy is now a very well known and essential tool for biological tissues characterization, its transposition to endomicroscopy remains problematic. Indeed, endomicroscopy requires several miniaturized elements like scanning system or distal lens of focalization (Ducourthial, 2013). The laser excitation, coming from a Ti: Sapph oscillator is classically delivered through an optical fibre, flexible and with a small diameter providing access to the internal hollow organs (alveoli, kidney…). The choice of the optimal fibre proves to be complex and must be realized taking into account all other parameters of the global system. The fibre has to be preceded by a shaping module for the compensation of linear and nonlinear effects occurring inside this material medium (Lelek 2007).

Currently, all the miniaturized parts of the endomicroscope are problematic and prevent the multiphotonic endomicroscope commercialisation. This is particularly true for the distal lens. Named "GRIN lenses" for gradient index lenses this technology is based on the gradient of negative refractive index of its material from the centre to its outskirts, glued inside a cylinder of stainless steel. Dimensions of classical GRIN lenses range between 0.35 to 2 mm in diameter and between 5 mm and few cm in length, with a numerical aperture (NA) of the object space between 0.2 and 0.8.

In this paper we present our study of GRIN lenses in the context of the development of a multiphotonic endomicroscope. The first part is dedicated to the experimental study of a GRIN lens alone. Background fluorescence induced in the GRIN lens is studied under UV excitation beam, mimicking the emitted multiphotonic fluorescence or second harmonic generation coming from biological samples. Then, the impact of the background fluorescence of the GRIN lens on its imaging ability, spectral detection and fluorescence lifetime measurements is evaluated. The 2D lateral resolution is experimentally measured using 1 µm diameter gold beads. The second part of the paper is dedicated to numerical simulations, using Zemax, of the GRIN lens coupled to a specifically designed double clad fibre (DCF) ideal for the assembly of a multiphotonic endomicroscope (Lefort, 2014). Both geometric ray tracing and Gaussian beam approach

were considered. Furthermore, the influence of the relative position between the GRIN lens and the DCF tip on the magnification, FOV, axial and lateral resolutions is evaluated. Finally, choosing a piezoelectric (PZT) stage as scanning device (Myaing, 2006), the coupling of the DCF with the PZT and the GRIN lens is characterized through the variation of the image working distance, the coupling efficiency of the fluorescence beam inside the DCF, the size of the field of view (FOV) and the axial and lateral resolutions.

2 GRIN LENS EXPERIMENTAL CHARACTERIZATION

2.1 GRIN Lens Definitions

The GRIN lenses are all manufactured with a medium having a continuously variable index of refraction between the periphery and the centre of the lens. This optic is glued to a biocompatible ring of stainless steel.

In this study, we have chosen to characterize a commercial GRIN lens (GT-MO-080-018-810, Grintech, Jena, Germany), with a total length of 7.53 mm and a diameter of 1.4 mm. Figure 1 shows the definitions of the image and object space and their working distances (WD). The object space contains the target biological sample and in the image space lies the DCF delivering the NIR excitation beam and collecting the multiphotonic signal emitted by the biological sample.
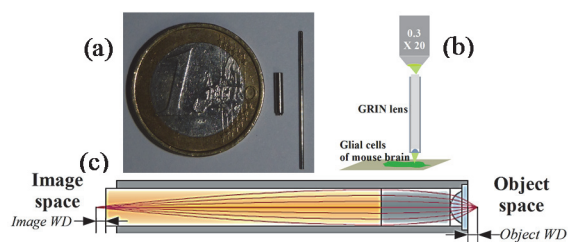

Figure 1: a. Picture of the two GRIN lenses. b. Setup for GRIN lens characterization from Grintech. c. Definitions of the image and object spaces and the corresponding WD.

2.2 Background Fluorescence

2.2.1 Imaging the Background Fluorescence

Fluorescence imaging techniques need a previous characterization of all the potential background source of fluorescence, as the GRIN lens. To start the characterization of the background fluorescence,

the GRIN lens is placed under the microscope objective of a confocal microscope focusing a krypton argon laser (Figure 1b). In this configuration, the confocal microscope gives an image of the image face of the GRIN lens Figure 2 presents the resulting observation of the image space of the GRIN lens.
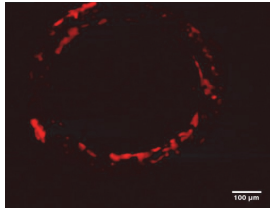

Figure 2: Fluorescence image of the glue between the GRIN lens and the stainless steel of protection by confocal imaging.

The inhomogeneous fluorescence signal from Figure 2 probably result from fluorescent components in the glue used to fix the GRIN lens to the steel ring. No impact of the intrinsic fluorescence of the glue on fluorescence images of biological samples was observed.

2.2.2 Spectroscopic Analysis

The background fluorescence of the GRIN lens is spectrally characterized. Figure 3 gives a representation of the experimental setup.
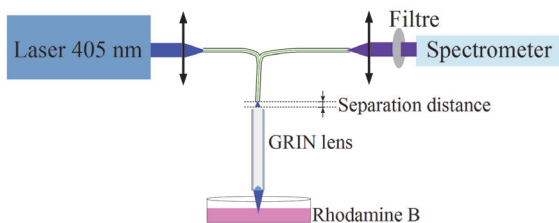

Figure 3: Experimental setup for the spectral characterization of the background fluorescence of the GRIN lens.

This setup consists of a pulsed diode laser from Picoquant at 405±10 nm (LDHP-C-405B, Picoquant) coupled into one of the two fibres of a bifurcated fibre. The laser power can be adjusted, as well as the repetition frequency, which can be set between 2.5 and 40 MHz The fibre guides the excitation laser source to the GRIN lens image space. A solution of Rhodamine B (RhB) is placed in the object space of the GRIN lens. The backward fluorescence, emitted by both the RhB and the GRIN lens, is collected by the second core of the bifurcated fibre and delivered to a spectrometer, preceded by a

long pass filter to reject the excitation laser beam. In a first stage the GRIN lens is excited with 405 nm laser source without the sample of RhB and without the filter to measure the background fluorescence emitted by the GRIN lens itself. The graph of Figure 4a is the emission spectrum of the background fluorescence. It can be seen that this spectrum covers a wide spectral range (around 400-700 nm).

The solution of RhB is then illuminated and its fluorescence emission spectrum was collected by the GRIN lens with a separation distance between the lens and the fibre of 2 mm and less than 200 μm (Figures 4b and 4c, respectively). Figures 4d and 4e present the analysis of the total spectrum by comparison with the spectrum obtained by the sum of the fluorescence spectra of the glue of the GRIN lens and the RhB solution. The latter was measured using the bifurcated fibre alone so as to eliminate its possible contribution to the fluorescence signal.
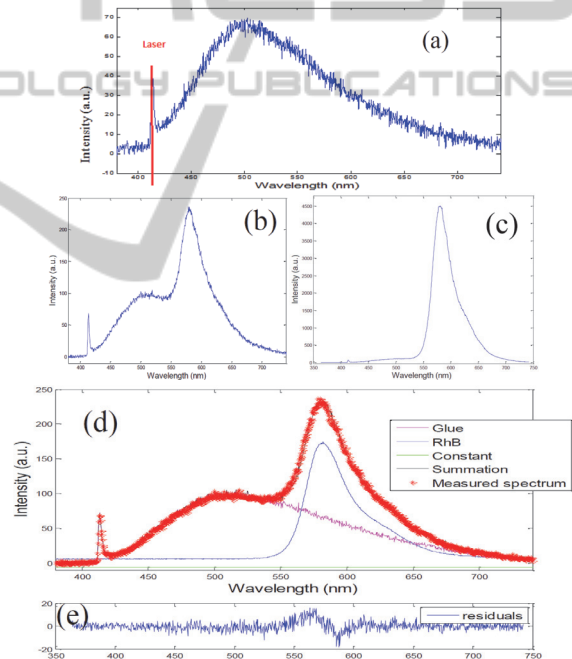

Figure 4: a. Emission spectrum of the background fluorescence induced by the GRIN lens alone with a 405 nm laser excitation. b. RhB fluorescence emission spectrum measured with a separation distance between the fibre and the GRIN lens of 2mm and c. of less than 200 μm. d. Summary of the measured emission spectra and the sum of the RhB and glue emission spectra. e. Calculation of the difference between the sum of each spectral component and the effective measured spectrum.

The contribution of the fluorescence from the glue around the GRIN lens is now spectrally characterized (Figures 4a, 4b and 4d). From

comparison between figures 4b and 4c, it can be shown that depending on the separation distance between the fibre tip and the GRIN lens, the contribution of the glue fluorescence is variable. At a large separation distance between the GRIN lens and the fibre tip (2 mm), the background fluorescence significantly altered the RhB spectrum, while the background fluorescence is hardly noticeable when this separation distance is very short, below 200 μm. This can be explained if one considers the very short image space WD of the GRIN lens (below 100 μm in air at 405 nm). It is also remarkable from Figure 4d that the RhB spectrum in blue recovers successfully the measured spectrum using the GRIN lens. Figure 4e corroborates this observation.

2.2.3 Lifetime Measurements with GRIN Lens

The two previous sections have brought out the presence of a background fluorescence perturbing the spectral measurement or the imaging through the GRIN lens in specific conditions. This section aims to present the effect of the GRIN lens position, in ideal conditions of object and image WD, on the measurement of fluorescence lifetime in time domain of the RhB.

To do so, the spectrometer of the setup described in Figure 3 is replaced by a photomultiplier tube (PMT) and a Time-Correlated Single Photon Counting (TCSPC) module synchronized with the excitation laser source. This method detects the exponential decay of fluorescence based on an accurate record of a single photon using a highly sensitive photon detector. The delay time of emission of a photon relative to the laser excitation pulse corresponds to the time spent in the excited state. Then, excitation is repeated several times to maintain the condition that only one photon per molecule is detected at each pulse. These measurements are recorded as a photon counting histogram representing the fluorescence decay time and the instrument response function (IRF), using a Time Harp 200 acquisition card (Pico- quant, Berlin Germany). The IRF characterizes the timing precision of TCSPC system and for an ideal system it should be infinitely narrow. During spectral or lifetime measurement the laser emission was rejected using a 410 nm high pass filter from (SR410, Semrock, USA) in order to detect fluorescence. The lifetime decays were fitted to an exponential model in order to extract the lifetime information with a reasonable fit quality, assessed

by the residuals of the fitting. An exponential model was chosen because it gives a good description of the physics involved in the lifetime decay. Two exponential models were tested to extract the lifetime information: the multi-exponential tail fit (no consideration of the IRF) and the exponential reconvolution (taking into account the IRF) detailed in equations (1) and (2).

$$I(t) = \sum_{i=1}^{n} A_i e^{-\frac{t}{\tau_i}} \quad (1)$$

$$I(t) = \int_{\infty}^{t} IRF(t') \sum_{i=1}^{n} A_i e^{-\frac{t-t'}{\tau_i}} dt' \quad (2)$$

Where:

I (t) represent the measured decay data,

A_i – amplitude of the ith component, in counts,

τ_i – lifetime of the ith component that has to be calculated.

IRF was measured using a mirror instead of the RhB sample and the filter was replaced by an optical density filter in order to let the attenuated laser beam pass to the PMT for IRF detection. The IRFs measurements of the fibre alone, the fibre coupled to a 10x microscope objective and the fibre coupled to the GRIN lens are shown and compared in Figure 5.
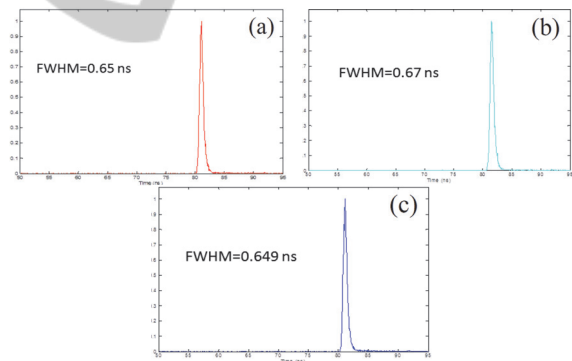

Figure 5: Lifetime measurements. a. Fibre alone. b. Fibre and objective 10x. c. Fibre and GRIN lens.
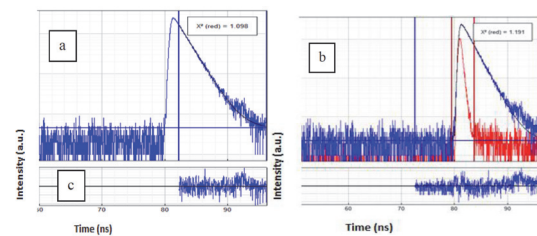

Figure 6: Measured fluorescence decay (in blue) and fitting model (in black). a. Lifetime of RhB without considering the IRF. b. Lifetime fitting by reconvolution, IRF deconvoluted with the decay data (in red). c. Residuals randomly distributed across the fitting range.

The IRFs are similar in the three conditions, with a FWHM around 0,65 ns. This proves that the GRIN lens does not affect lifetime measurements.

Lifetime measurements and decay fits of the fluorescence signal of the RhB solution were then realized, using the two fitting methods previously detailed. Figures 6a and 6b present the results of fluorescence lifetime measurements of RhB with the fitting curves.

The results of lifetime decays of RhB through the different elements of the setup are summarized in the Table 1.

Table 1: Lifetime decay fitting through the setup elements using tail fitting without the IRF and reconvolution fitting with the IRF.

Element of the setup	Fit method	A (counts)	τ (ns)
Fibre	Tail	1872.4±20.9	1.72±0.02
	Reconv	14046 ± 94.7	1.67 ± 0.01
Objective	Tail	1638.5 ± 19.3	1.705 ± 0.015
	Reconv	3345.3 ± 40.4	1.703 ± 0.014
GRIN lens	Tail	252.5 ± 9.41	1.628 ± 0.049
	Reconv	1835 ± 29.6	1.616 ± 0.019

In the literature (Boens 2007), the mean lifetime data of the fluorescence lifetime of a solution of RhB in water at 20°C is

$\tau_{RhB,ref}$ = 1.72±0.02 ns. The fluorescence lifetime is therefore not affected by the presence of the fibre considering the tail fitting method, while the reconvolution method is less relevant. Furthermore, the fluorescence lifetime is not significantly disturbed by the microscope objective if one takes the experimental incertitude into account. Finally, it can be seen that for the GRIN lens, both fitting methods, lead to a decrease of the fluorescence lifetime from 1.7 ns to about 1.62 ns. This may be explained by the detection of fluorescence signal of the glue of the GRIN lens, leading to an average measurement of the lifetime of the RhB and the glue. That point corroborates the previous conclusions in section 2.2.1 and 2.2.2 on the significant perturbation of the signal collected by the GRIN lens due to the background fluorescence of the glue.

2.3 GRIN Lens Resolution

The resolution of the whole imaging system (10x microscope objective + GRIN lens) is characterized using 1μm diameter gold beads through the confocal microscope. Those beads are assumed to be point sources and the axial and lateral profiles of their images are fitted by a Gaussian function depicted in Figures 7a, 7b and 7c. The fitting was applied in order to calculate the full width half maximum (FWHM), considered as the optical resolution of the system.
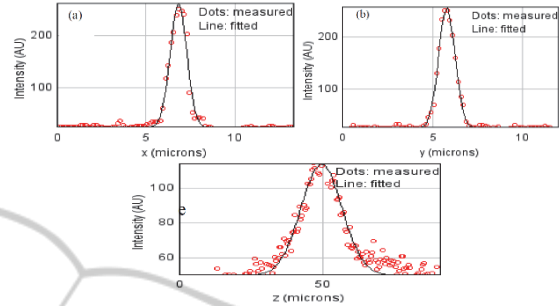

Figure 7: Beads profile measurements and their Gaussian fits. a. Lateral resolution in x (μm). b. Lateral resolution in y (μm). c. Axial resolution in z (μm).

The lateral resolution is 1 μm in x and 1 μm in y, in good agreement with the best performances described in the literature (Gu, 2014).

3 NUMERICAL SIMULATIONS

A numerical simulation of the GRIN lens in the context of the manufacturing of an optimized nonlinear endomicroscope is proposed. These simulations are led simultaneously for NIR nonlinear excitation and collection of the multiphotonic signal emitted by the target. The GRIN lens is coupled to the scanning system and the optical fibre. The simulated fibre, a DCF, delivers the nonlinear excitation by the core and collects the multiphotonic emission by the inner cladding. This DCF is simulated with ideal parameters for delivering the multiphotonic excitation through a small core diameter (5 μm) single mode at 800 nm with a small NA (0.04) and a large inner cladding diameter (200 μm) to collect the maximum of multiphotonic signal from the GRIN lens thanks to a large NA (0.3).

3.1 Simulation of the PZT Scanning

The scanning system is a tubular piezoelectric scanner (PZT). This device consists in a small tubular piezoelectric actuator governed by four electrodes grouped in two pairs, with an optical fibre positioned inside the actuator and electrically glued at its tip. This layout allows driving the fibre tip, exceeding the PZT for several tens of millimetres by

application of a specific waveform (triangular or sinusoidal) with a specific frequency, for each pair of electrodes. This results in a circular scanning pattern of the extremity of the fibre. The amplitude is adjustable so that the position of the fibre tip can be set on all the surface of a circle. The focalization of the excitation beam on different parts of the target relies on the relative position of the fibre with the GRIN lens, as illustrated in Figure 8.

Figure 8: Complete scheme of the endomicroscope distal end containing the DCF to guide the excitation and collection signals, the PZT for scanning and the GRIN lens for the focalization and the collection.

The use of the PZT scanning system on the fibre tip imposes an angle between the fibre tip and the GRIN lens, resulting in several consequences. First of all, the object WD varies in function of the fibre angle. Moreover, the coupling efficiency between the excitation beam and the GRIN lens, linked to the DCF core diameter and its NA is necessarily modified by the tilt angle of the DCF. Figures 9a and 9b resume the related simulations.
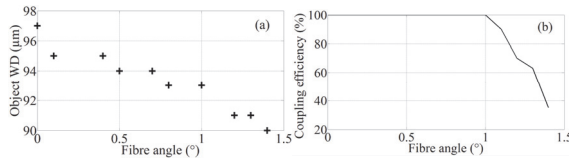

Figure 9: a. Evolution of the object WD with the inclination of the fibre tip due to the PZT scanning system. b. Evolution of the coupling efficiency of the excitation beam with the DCF angle.

Figure 9a shows a decrease of the object WD with the fibre angle, revealing the fact that the fibre tip is not really a plan, but a semi-sphere. This parameter is not a major drawback but it should be considered for the interpretation of the obtained images. Concerning the coupling efficiency between the excitation beam and the GRIN lens (Figure 9b), an increase of the fibre angle leads to an important decrease of the coupling. Indeed, 10% are lost for an angle of 1.1° and more than 60% are not coupled for 1.4°. A direct consequence of this situation is the reduction of the field of view in the object space.

It can be noticed that the PZT scanning system is interesting by its small diameter ideal for a distal end miniaturization. But several perturbations on the detected image have to be taken into account to interpret the images.

3.2 Optimization of the Distance between the DCF and the GRIN Lens

The separation distance between the DCF and the GRIN lens is a critical parameter. Indeed, the focal point position and thus the object WD, the magnification properties, the coupling efficiency and the field of view (FOV) are the main parameters that may vary with this distance. They are simulated here and the results are summarized in Figure 10 for a distance ranging between 0 mm and 3 mm.
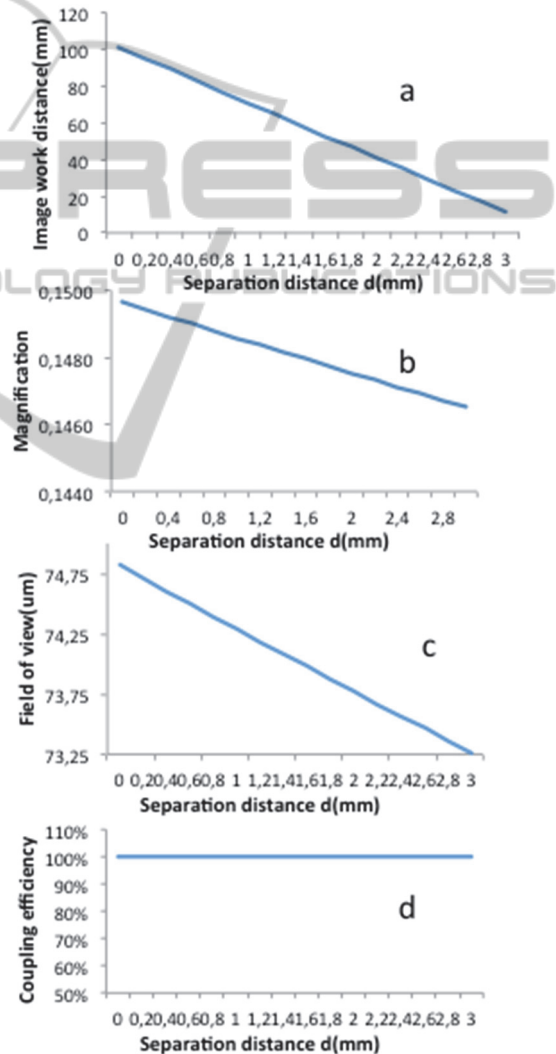

Figure 10: Numerical simulations of the influence of the separation distance between the fibre tip and the GRIN lens on several parameters. a. Object WD. b. Magnification. c. FOV. d. Coupling efficiency.

As expected, the object WD decreases when the separation distance between the fibre and the GRIN

lens increases. Consequently, the focal point is under control of this parameter and can be adjusted between 10 and 100 μm, the highest penetration depth reachable by the excitation beam. The magnification and the FOV decrease slowly when the separation distance increases. For example, the FOV, which is very small at the origin (less than 75 μm) declines to about 73.25 μm at 3 mm

Finally, the coupling efficiency of the multiphotonic signal emitted by the sample after the collection by the GRIN lens is not modified whatever the distance between the fibre and the GRIN lens. This results from the big inner cladding diameter of 200 μm with the highest possible NA of 0.3. That optimized parameter is crucial for the efficient collection of very weak multiphotonic endogenous signals.

To conclude, these simulations show that if an axial scanning is needed, moving the separation distance between the fibre and the GRIN lens is a way to operate. Nevertheless, one has to expect an important decrease of the object WD as well as a modification of the magnification and the FOV.

4 CONCLUSIONS

In the context of the miniaturization of a distal head of an endomicroscope, GRIN lenses are commonly used. The aim of this article is to characterize a commercial GRIN lens. The performances of the GRIN lens to make images of brain tissues were tested under a confocal microscope. The presence of a fluorescent signal emitted by the outlying glue all around the effective area of the lens was revealed, and the imaging of glial cells of mouse brain showed no influence on the resulting fluorescent image of the sample. Starting from this observation, the importance of this background fluorescence was evaluated by spectral analysis and fluorescence lifetime measurements. Both of them were showing a non-negligible part of this fluorescence that can be easily identified by its spectrum and by its lifetime.

The GRIN lens resolutions were then established to around 1 μm for lateral resolution and 16 μm for axial resolution, in accordance with the values usually presented in the literature.

Finally, numerical simulations of an endomicroscope including this GRIN lens coupled to a homemade DCF fixed with a PZT scanning system were led. The limitations of the use of this PZT were highlighted: the focal plan is necessarily not plan but curved and the coupling efficiency of the excitation beam between the DCF and the GRIN

lens is dramatically reduced to less than 40% of coupling when the fibre angle exceeds 1.4°. Furthermore, the separation distance between the DCF and the GRIN lens influenced the position of the focal point in the object plan. This observation presents a way to perform an axial scanning system, which is still a limiting point for obtaining 3D images. Nevertheless, a modification of the separation distance induces a reduction of the FOV and of the magnification. The best simulated FOV obtained with the GRIN lens is 75 μm square, very small and far from the ideal situation usually asked by the surgeons of 1 mm square.

All these limitations have to be carefully thought for the experimental use of the GRIN lens. It remains that GRIN lens technology is the only one allowing a distal lens with a diameter smaller than 0.5 mm, a decisive advantage in nonlinear endomicroscopy.

ACKNOWLEDGEMENTS

REFERENCES

Cosignani, V., Dvornikov, A., Aguilar, J.-S., Stingari, C., Edwards, R., Mantulin, W. W., Gratton, E., 2012. *Deep tissue fluorescence imaging and in vivo biological applications*. Journal of Biomedical Optics, 17, 11, 116023.

Ducourthial, G., Lefort, C., Peyrot, D.A., Mansuryan, T., Kruglik, S.G., Vever-Bizet, C., Thiberville, L., Lacombe, F., Bourg-Heckly, G., Louradour, F., 2013. *Label free multiphoton imaging of human pulmonary tissues through two-meter-long microstructured fiber and multicore image-guide*. Progress in Biomedical Optics and Imaging - Proceedings of SPIE, 85750H.

Gu, M., Bao, H., Kang, H., 2014. *Fibre-optical microendoscopy*. Journal of Microscopy, 254, 1, pp. 13-18.

Kim, J., Lee, W. M., Kim, P., Choi, M., Jung, K., Kim, S., Yun, S. H., 2012. *Fabrication and operation of GRIN probes for in vivo fluorescence cellular imaging of internal organs in small animals*. Nature Protocols, 7, 8, pp 1456-1469.

Lefort, C., Hamzeh, H., Louradour, F., Pain, F., Abi Haidar, D., 2014. *Characterization, comparison and choice of a commercial double-clad fiber for nonlinear endomicroscopy*. Journal of Biomedical Optics, 19, 7, 076005.

Lelek, M., Suran, E., Louradour, F., Barthelemy, A., Viellerobe, B., Lacombe, F., 2007. *Coherent femtosecond pulse shaping for the optimization of a non-linear micro-endoscope*. Optics Express, 15, 16, pp 10154-10162.

Miller, A. B., Hoogstraten, B., Staquet, M., & Winkler, A. 1981. *Reporting results of cancer treatment*. Cancer, 47(1), 207-214.

Myaing, M. T. M., MacDonald, D. J., Li, X., 2006. Fiber-optic scanning two-photon fluorescence endoscope. Optics Letters, 31, 8, pp 1076-1078.

Salaün, M., Roussel, F., Hauss, P.-A., Lachkar, S., Thiberville, L., 2010. *In vivo imaging of pulmonary alveolar proteinosis using confocal endomicroscopy*. European Respiratory Journal, 36, 2, pp 451-453.

Wang, T., Li, Q., Xiao, P., Ahn, J., Kim, Y.E., Park, Y., Kim, M., Song, M., Chung, E., Chung, W.K., Ahn, G.-O., Kim, S., Kim, P., Myung, S.-J., Kim, K.H., 2014. Gradient index lens based combined two-photon microscopy and optical coherence tomography, Optics Express, 22, 11, pp 12962-12970.